Građevinski materijali i konstrukcije
Building Materials and Structures
journal homepage: www.buildingmaterialsstructures.com

http://doi.ogr/10.5937/GRMK2500014M

Original scientific paper

Layerwise theory-based finite elements for static and dynamic analysis of CLT-concrete composites with partial shear connection

Miroslav Marjanović*[1)]

[1)] *University of Belgrade – Faculty of Civil Engineering, Bulevar kralja Aleksandra 73, 11000 Belgrade, Serbia*

Article history

Received: 20 October 2025
Received in revised form: 04 December 2025
Accepted: 08 December 2025
Available online: 22 December 2025

Keywords

timber-concrete composite,
cross-laminated timber,
layered finite element,
layerwise theory

ABSTRACT

The paper presents a formulation of layered finite elements (based on Reddy's full-layerwise-theory) for static and dynamic analysis of cross-laminated-timber concrete composites (CCC). A partial interaction between concrete and cross-laminated-timber (CLT), allowing for interlayer slip, is incorporated by using distributed elastic springs in the CLT-concrete interface. A linear discontinuous layer-wise interpolation of displacement components through the thickness is imposed to account for complex layerwise kinematics including partial shear connection.

The model is implemented using the original MATLAB framework, while the graphical user interface is developed in GiD environment. It is validated against the available data in the literature, and excellent agreement for static and dynamic simulations is obtained with computational cost savings. The complex 3D displacement/strain/stress fields and natural frequencies of the CCC with various interlayer slip moduli are accurately predicted. The parametric study on the influence of partial shear connection on stress distribution within the CCC is provided as a benchmark for future investigations. The developed model can be applied for the analysis of timber-concrete (TCC) or other plate-like layered composites with partial shear connection and arbitrary geometry.

1 Introduction

The advantages of cross-laminated timber for the building sector are mainly related to its low environmental impact, high mechanical performance, ease of prefabrication and short erection time on site [1, 2]. The above encourage the use of CLT in modern residential and commercial buildings instead of traditional mineral-based materials. CLT provides the considerable stiffness with the low weight, allowing the application of such panels as full-size walls or floors, suitable for loading in-plane and out-of-plane, while the crosswise layer orientation ensures uniform shrinkage and swelling properties [3]. To further increase the application of CLT, CLT-concrete composites (CCC) gained extensive application in floor systems in recent years because of their unique and outstanding performance, by means of stiffness, bending resistance, good dynamic behavior and superior sound and thermal insulation [4-6]. These composites provide a prominent alternative to the conventional reinforced concrete (RC) floors in medium- to high-rise buildings, and present the logical continuation in the development of timber-concrete composites (TCC) [7-9].

In TCC and CCC, the timber and concrete layers are interconnected using different connection systems: notched shear connectors [10-13], screwed connectors [14-15], mechanically attaching dowel-type fasteners [16], adhesives and gluing with rods [17-18], shear studs [19-20], or a combination of various fastening systems. The choice of connection is important due to the structural rigidity under service load, vibration performance and stiffness during a fire. Each connection system requires distinctive types of arrangements and possesses unique characteristics. The adhesive connection provides high stiffness and uniform distribution of the forces and low slip over the entire composite, while the shear connectors of different types are used to create a path for transfer shear forces between the concrete slab and CLT layer. Remarkable efforts have been invested so far to predict the slip modulus and shear capacity of the screwed connections, associated with different concrete, timber, and insulation thicknesses, concrete and timber properties and screw sizes, layouts, and penetration lengths. Extensive experimental programs followed by the development of analytical solutions for the prediction of slip modulus and interlayer slip have been conducted so far [21-25].

CLT floors and their composites are prone to excessive vibrations due to human activities [26, 27], which are the most common vibration sources in residential and commercial buildings. Excessive vibrations can be detrimental to occupants' comfort or may cause malfunctions

* Corresponding author:
E-mail address: mmarjanovic@grf.bg.ac.rs

of vibration-sensitive equipment [28]. Consequently, design of long-span open-plan CLT floors is commonly governed by vibration serviceability requirements rather than strength and deflection limits [29, 30]. Having in mind that recent research of Mohammed et al. [31] showed that the resonant vibration response in floors can occur even at frequencies as high as 14 Hz, the structural design for serviceability limit state by means of vibration must be performed with particular attention. The above requires accurate computational models, which may account for specifics of such structures, such as transverse shear deformation and partial shear connection at the interface. Guo et al. [32] examined the effect of a floating concrete topping on the vibration performance and dynamic characteristics of mass timber slab floors through experimental tests, determined the effective flexural stiffness of the floor systems and developed finite element models to accurately predict the modal properties. Bao et al. [33] predicted the vibration performance of CCC floor strips using theoretical calculations and finite element simulations, and conducted the parametric numerical analyses using the analytical methods to determine the optimal section thickness ratio between CLT and concrete, while Malek et al. [34] provided the important data on mass timber floor system performance in furnished office buildings.

Current computational models for the prediction of static and dynamic response CLT-concrete composites mainly emerged from the long tradition of using only simple beam-like theoretical approaches, which are limited to account for two-dimensional load transfer and cannot reflect the load carrying mechanism of a plate-like structure [35]. Two-dimensional approaches are applied through the applications of equivalent-single-layer (ESL) laminate theories [36-40], with the appropriate shear correction factors [41]. ESL theories consider the displacements as continuous functions of the thickness coordinate. This assumption cannot be satisfied at the CLT-concrete interface within the CCC, since a completely rigid connection between CLT and concrete is typically not achieved. Therefore, as shown in [42], the partial shear connection must be taken into account. This may be achieved by the use of the equivalent-layer zig-zag kinematics based on the Lekhnitskii's [43] and Ren's models [44, 45]. Furtmüller has recently extended the formulation for TCC beams [46] and plates [42], to predict the static and dynamic response of TCC and CCC. The mentioned formulation requires the a priori assumption of the location of the neutral axis within the TCC or CCC, and provides the computationally effective alternative to the conventional (solid) finite element models, without the necessity for shear correction factors. In addition, Ladurner et al. captured the geometrically nonlinear response of slender symmetrically layered beams while simultaneously capturing the effects of variable cross-section and interlayer slip [47].

It was recently showed that Full-Layerwise Plate Theory of Reddy (FLWT) [48] can provide the accurate results for CLT panels in bending [35, 49], without compromising the accuracy of the 3D models. This theory incorporates the transverse normal stress σ_z and accounts for continuous transverse (interlaminar) stresses τ_{xz}, τ_{yz} and σ_z at layer interfaces within a CLT, without the use of shear correction factors. Although the zig-zag theories provide the adequate balance between ESL and layerwise theories, the FLWT provides the possibility to account for localized effects, such as holes or cut-outs and provides the complete stress field necessary for failure analysis or delamination studies. The mentioned FLWT formulation is extended in this paper to also account for the interlayer slip at the CLT-concrete interface. The slip moduli are incorporated using the smeared approach, as distributed linear springs in three orthogonal directions at the interface. Based on the presented formulation, a family of layered quadrilateral isoparametric finite elements has been developed. The computational model is implemented within the original object-oriented code FLWTFEM [50, 51] coded in MATLAB [52] and connected with the pre- and post-processing software GiD [53]. The presented approach is validated against the available data in the literature, based on the zig-zag theory and results from the 3D models in Abaqus CAE [54]. Excellent agreement for static and dynamic simulations is obtained with computational cost savings. Finally, a parametric study on the influence of interlayer slip modulus on stress distribution in CCC is provided as a benchmark for future investigations. The model flexibility allows, in a similar manner, the analysis of timber-concrete (TCC) or other plate-like layered composites with partial shear connection and arbitrary geometry. As shown in [51], the layered triangular elements may be developed analogously.

The paper is organized as follows: after the introduction, the governing equations of the full-layerwise theory, its extension to account for the partial interaction and the corresponding FLWT-based finite element model are presented in Section 2. Model validation is elaborated in Section 3, while the conclusions and recommendations for further research are given in Section 4.

2 Layerwise formulation of CLT-C kinematics and finite element implementation

2.1 Kinematics

In the paper, a CLT-concrete composite plate made of n_{CLT} orthotropic layers and a concrete (isotropic) topping is considered. The CLT thickness is denoted as h_{CLT} (see Figure 1), the concrete topping thickness is denoted as h_C, while the thickness of the k^{th} lamina (including both CLT and concrete layers) is denoted as h_k (k = 1, 2,…, n). The plate is loaded with $q_t(x,y,h)$ and $q_b(x,y,0)$ acting to either top or the bottom surface (S_t or S_b).

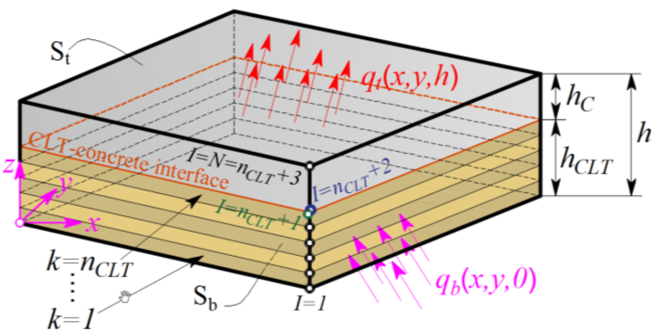

Figure 1. CLT-concrete composite plate with $n_{CLT}+1$ material layers and $N=n_{CLT+3}$ numerical layers (interfaces). $I=n_{CLT}+1$ is the top numerical layer of the CLT, while $I=n_{CLT}+2$ is the bottom numerical layer of the concrete.

Piece-wise linear variation of all three displacement components through the plate thickness is imposed, leading to the 3D stress description of all material layers. The displacement field (u, v, w) of an arbitrary point (x,y,z) of the CLT-C composite is given as:

$$u(x,y,z)=\sum_{I=1}^{N}U^{I}(x,y)\Phi^{I}(z),\quad v(x,y,z)=\sum_{I=1}^{N}V^{I}(x,y)\Phi^{I}(z),\quad w(x,y,z)=\sum_{I=1}^{N}W^{I}(x,y)\Phi^{I}(z) \tag{1}$$

where $U^I(x,y)$, $V^I(x,y)$ and $W^I(x,y)$ are the displacement components in the I^{th} "numerical layer" of the plate in three orthogonal directions, respectively, while N is the total number of numerical layers. $\Phi^I(z)$ are selected to be linear layerwise functions of the z-coordinate [55], defined over the considered layer (above and below the numerical layer I). This selection implicitly defines the numerical layers in planes between the material layers, including S_t and S_b. Note that in an (zero-thickness) interface between the CLT and concrete topping, two independent numerical layers are introduced, which enables a relative displacement in all directions between the CLT and concrete. The above definition leads to the number of numerical layers $N = n_{CLT} + 3$, as shown in Figure 1.

Since only partial shear connection between CLT and concrete may be achieved, the relative displacements (interlayer slip) between the CLT and concrete arise [42]. Interlayer slips Δu, Δv and Δw, respectively, in the CLT-concrete interface, are introduced by means of different displacements in the numerical layers $n_{CLT}+1$ and $n_{CLT}+2$ located at the CLT-concrete interface (Figure 2a). By means of mathematical description, the inter-layer slip is enabled using the discontinuous interpolation functions $\Phi^{n_{CLT}+1}$ and $\Phi^{n_{CLT}+2}$ [55], as shown in Figure 2b. This leads to the discontinuous displacement fields (1), as shown in Figure 2c.

2.2 Stresses and strains

The linear strain field is inherited from the displacement field (1) and the layerwise interpolation shown in Figure 2b. The explicit expressions of the strain field (given in [48]) are extended by adding the following singularity terms related to the CLT-concrete interface (^{int}):

$$\gamma_{yz}^{\text{int}}=\Delta v(x,y,h_{CLT}),\quad \gamma_{xz}^{\text{int}}=\Delta u(x,y,h_{CLT}),\quad \varepsilon_{z}^{\text{int}}=\Delta w(x,y,h_{CLT}) \tag{2}$$

If the thermal contributions are neglected, the stresses in the k^{th} numerical layer may be computed from the lamina 3D constitutive equations [35, 48]:

$$\begin{Bmatrix}\sigma_x\\ \sigma_y\\ \sigma_z\\ \tau_{yz}\\ \tau_{xz}\\ \tau_{xy}\end{Bmatrix}^{(k)}=\begin{bmatrix}\bar{C}_{11}&\bar{C}_{12}&\bar{C}_{13}&0&0&\bar{C}_{16}\\ \bar{C}_{21}&\bar{C}_{22}&\bar{C}_{23}&0&0&\bar{C}_{26}\\ \bar{C}_{31}&\bar{C}_{32}&\bar{C}_{33}&0&0&\bar{C}_{36}\\ 0&0&0&\bar{C}_{44}&\bar{C}_{45}&0\\ 0&0&0&\bar{C}_{45}&\bar{C}_{55}&0\\ \bar{C}_{16}&\bar{C}_{26}&\bar{C}_{36}&0&0&\bar{C}_{66}\end{bmatrix}^{(k)}\begin{Bmatrix}\varepsilon_x\\ \varepsilon_y\\ \varepsilon_z\\ \gamma_{yz}\\ \gamma_{xz}\\ \gamma_{xy}\end{Bmatrix}^{(k)} \tag{3}$$

where $\bar{C}_{ij}$ are the transformed elastic coefficients in the (x,y,z) coordinates, which are related to the elastic coefficients in the material (1,2,3) coordinates (C_{ij}) through the transformation matrix $\mathbf{T}^{(k)}$ for the k^{th} layer. Matrices $\mathbf{T}^{(k)}$ are well-known and can be found in [48].

Note that for $k \le n_{CLT}$, the angle θ between the lamina (1,2,3) and the laminate (x,y,z) coordinate systems is either 0° or 90°, while for the concrete layer(s), θ can be arbitrarily selected (say 0°). For $k \le n_{CLT}$, the mentioned matrix $\mathbf{C}$ corresponds to the (orthotropic) timber material with 9 independent material constants E_{ij}, G_{ij} and ν_{ij}. The principal material axes of the timber are aligned with the fiber or trunk direction (L), and orthogonal to the annual rings (radial direction – R and tangential direction - T) [35]:

$$\mathbf{C}=\begin{bmatrix}C_{11}&C_{12}&C_{13}&0&0&0\\ C_{12}&C_{22}&C_{23}&0&0&0\\ C_{13}&C_{23}&C_{33}&0&0&0\\ 0&0&0&C_{44}&0&0\\ 0&0&0&0&C_{55}&0\\ 0&0&0&0&0&C_{66}\end{bmatrix} \tag{4}$$

where C_{ij} and Δ are given in Eq. (5).

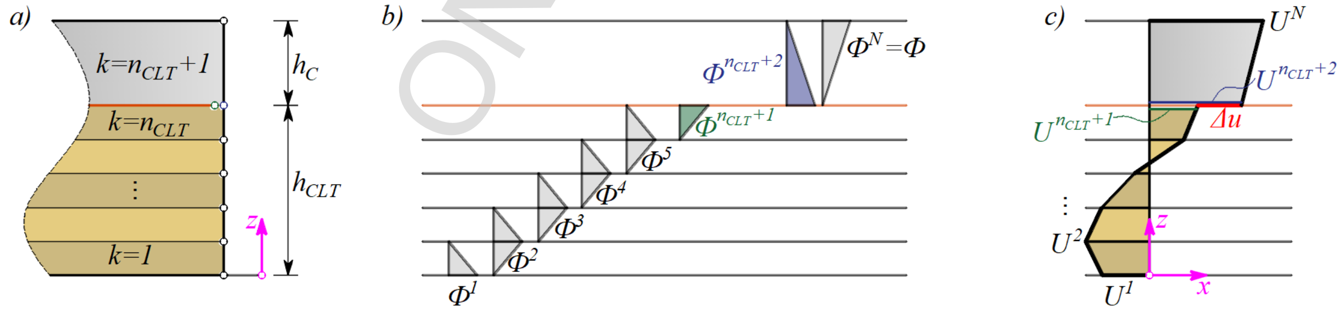

Figure 2. a) CLT-C composite with the interface at $z = h_{CLT}$; b) linear layerwise functions $\Phi^I(z)$ with a discontinuity at CLT-concrete interface; c) discontinuous displacement field (i.e. in x-direction) with marked relative displacement Δu

$$C_{11}=\frac{1-\nu_{RT}\nu_{TR}}{E_R E_T\Delta},\ C_{12}=\frac{\nu_{RL}-\nu_{TL}\nu_{RT}}{E_R E_T\Delta}=\frac{\nu_{LR}-\nu_{TR}\nu_{LT}}{E_L E_T\Delta},\ C_{13}=\frac{\nu_{TL}+\nu_{RL}\nu_{TR}}{E_R E_T\Delta}=\frac{\nu_{LT}+\nu_{LR}\nu_{RT}}{E_L E_R\Delta},\ C_{22}=\frac{1-\nu_{LT}\nu_{TL}}{E_L E_T\Delta},$$

$$C_{23}=\frac{\nu_{TR}+\nu_{LR}\nu_{TL}}{E_L E_T\Delta}=\frac{\nu_{R}+\nu_{RL}\nu_{LT}}{E_L E_T\Delta},\ C_{33}=\frac{1-\nu_{LR}\nu_{RL}}{E_L E_R\Delta},\ C_{44}=G_{RT},\ C_{55}=G_{LT},\ C_{66}=G_{LR}, \tag{5}$$

$$\Delta=\frac{1-\nu_{LR}\nu_{RL}-\nu_{RT}\nu_{TR}-\nu_{LT}\nu_{TL}-2\nu_{RL}\nu_{TR}\nu_{LT}}{E_L E_R E_T}$$

$$\mathbf{C}=\frac{E_c}{(1+\nu_c)(1-2\nu_c)}\begin{bmatrix} 1-\nu_c & \nu_c & \nu_c & 0 & 0 & 0 \\ \nu_c & 1-\nu_c & \nu_c & 0 & 0 & 0 \\ \nu_c & \nu_c & 1-\nu_c & 0 & 0 & 0 \\ 0 & 0 & 0 & \frac{1-2\nu_c}{2} & 0 & 0 \\ 0 & 0 & 0 & 0 & \frac{1-2\nu_c}{2} & 0 \\ 0 & 0 & 0 & 0 & 0 & \frac{1-2\nu_c}{2} \end{bmatrix} \tag{6}$$

On the other hand, for $k>n_{CLT}$, **C** corresponds to the concrete (isotropic) material properties given in Eq. (6). The interfacial stresses acting in the interface are proportional to the slip moduli K_i:

$$\begin{aligned} \tau_{xz}^{\text{int}} &= K_x\gamma_{xz}^{\text{int}} = K_x\Delta u(x,y,h_{CLT}), \\ \tau_{yz}^{\text{int}} &= K_y\gamma_{yz}^{\text{int}} = K_y\Delta v(x,y,h_{CLT}), \\ \sigma_z^{\text{int}} &= K_z\varepsilon_z^{\text{int}} = K_z\Delta w(x,y,h_{CLT}) \end{aligned} \tag{7}$$

Note that for a very high selected value of K_z (say 10^3 higher than K_x or K_y), the relative displacement Δw tends to zero which is a common value in CCC.

When the constitutive law on the lamina level is established, the constitutive relations of the CCC can be derived in a usual manner [48] by the explicit integration of the lamina constitutive equations (3) through the thickness of the laminate. This eliminates the thickness coordinate and reduces a 3D problem to a 2D one, which is a main advantage of the layerwise theory. Using the principle of virtual displacements, the system of 3*N* Euler-Lagrange governing equations of motion (strong form) of the FLWT are then derived by satisfying the equilibrium of the virtual strain energy ***δU***, the work done by the applied forces ***δV*** and the virtual kinetic energy ***δK***:

$$\begin{aligned} &\frac{\partial N_{xx}^I}{\partial x}+\frac{\partial N_{xy}^I}{\partial y}-Q_x^I=\sum_{J=1}^{N} I^{IJ}\ddot{U}^J, \\ &\frac{\partial N_{xy}^I}{\partial x}+\frac{\partial N_{yy}^I}{\partial y}-Q_y^I=\sum_{J=1}^{N} I^{IJ}\ddot{V}^J, \\ &\frac{\partial Q_x^I}{\partial x}+\frac{\partial Q_y^I}{\partial y}-\tilde{Q}_z^I+q_b\delta_{I1}+q_t\delta_{IN}=\sum_{J=1}^{N} I^{IJ}\ddot{W}^J \end{aligned} \tag{8}$$

In (8), $N_{xx}^I, N_{xy}^I, N_{yy}^I, Q_x^I, Q_y^I, \tilde{Q}_z^I$ are stress resultants in the I^{th} numerical layer defined in [48]; δ_{I1} and δ_{IN} are displacement vectors at the S_b and S_t, respectively, $\ddot{U}^J, \ddot{V}^J, \ddot{W}^J$ are second derivatives with respect to time (*t*), while I^{IJ} is the mass moment of inertia calculated as ($\rho^{(k)}$ denotes the mass density of the k^{th} layer):

$$I^{IJ}=\sum_{k=1}^{n}\int_{z_k}^{z_{k+1}}\rho^{(k)}\Phi^I\Phi^J dz \tag{9}$$

Note that beside the formulation presented in [35], the additional term enters the principle of virtual work, originating from the interfacial shear stresses at the interface (int):

$$\delta U^{\text{int}}=\int_{\Omega}\int_{0}^{h_{CLT}+h_C}\tau_{xz}^{\text{int}}\delta\gamma_{xz}^{\text{int}}+\tau_{yz}^{\text{int}}\delta\gamma_{yz}^{\text{int}}+\sigma_z^{\text{int}}\delta\varepsilon_z^{\text{int}}dzd\Omega \tag{10}$$

The first term in the previous integral (10) is given in Eq. (11). By analogy, the same applies for the remaining two terms in the integral (10).

2.3 Finite element model

Based on the above formulation, the family of 2D finite elements is derived by substituting an assumed interpolation of the displacement field (1) into the equations of motion of the FLWT. All displacement components are interpolated using the same degree of interpolation, as shown in Eq. (12). Note that in Eq. (12), *m* is the number of element nodes in the 2D element (note that out-of-plane coordinate has been previously eliminated). In addition, U_j^I, V_j^I, W_j^I are the nodal values of displacements U^I, V^I and W^I, respectively, in the j^{th} node of the 2D element (representing the kinematics in the I^{th} numerical layer), while $\psi_j(x,y)$ are the 2D Lagrange shape functions associated with the j^{th} element node.

The 2D data structure similar to the plate-like FE models provides several advantages against the conventional 3D models [35]: reduced input data, independent interpolation of in- and out-of-plane displacements, and computational savings in numerical integration.

$$\begin{aligned} \delta U_x^{\text{int}} &= \int_{\Omega}\int_{0}^{h_{CLT}+h_C}\tau_{xz}^{\text{int}}\delta\gamma_{xz}^{\text{int}}dzd\Omega=\int_{\Omega}\int_{0}^{h_{CLT}+h_C}K_x\left(u_{n_{CLT}+2}-u_{n_{CLT}+1}\right)\left(\delta u_{n_{CLT}+2}-\delta u_{n_{CLT}+1}\right)dzd\Omega \\ \delta U_x^{\text{int}} &= \int_{\Omega}\int_{0}^{h_{CLT}+h_C}\left(\begin{bmatrix}\delta u_{n_{CLT}+1} & \delta u_{n_{CLT}+2}\end{bmatrix}_{1\times 2}\begin{bmatrix}K_x & -K_x \\ -K_x & K_x\end{bmatrix}_{2\times 2}\begin{bmatrix}u_{n_{CLT}+1} \\ u_{n_{CLT}+2}\end{bmatrix}_{2\times 1}\right)dzd\Omega \end{aligned} \tag{11}$$

$$U^I(x,y)=\sum_{j=1}^{m}U_j^I\psi_j(x,y),\quad V^I(x,y)=\sum_{j=1}^{m}V_j^I\psi_j(x,y),\quad W^I(x,y)=\sum_{j=1}^{m}W_j^I\psi_j(x,y) \tag{12}$$

The matrix form of the finite element model is obtained as:

$$\left[K^{IJ}\right]\left\{\Delta^{J}\right\}+\left[M^{IJ}\right]\left\{\ddot{\Delta}^{J}\right\}=\left\{F^{J}\right\} \tag{13}$$

where $[K^{IJ}]$ and $[M^{IJ}]$ are the element stiffness and mass matrices, respectively; $\{\Delta^J\}$ and $\{\ddot{\Delta}^J\}$ are the element displacement and acceleration vectors, respectively, while $\{F^J\}$ is the element force vector (I=1,…,N and J=1,…,N).

In the element stiffness matrix, the additional terms K_x, K_y and K_z corresponding to the interlayer slip moduli in three orthogonal directions are added in the rows and columns corresponding to the total of 6m nodal displacements in the CLT-concrete interface: $U_i^{n_{CLT}+2}, U_i^{n_{CLT}+1}, V_i^{n_{CLT}+2}, V_i^{n_{CLT}+1}$, $W_i^{n_{CLT}+2}$ and $W_i^{n_{CLT}+1}$. The additional term related to the interface (int) is calculated over the finite element domain Ω_e as:

$$\left[\mathbf{K}^{\text{int}}\right]_{6m\times 6m}=\int_{\Omega_e}\left(\begin{matrix}\left[\mathbf{B}_1\right]^T\begin{bmatrix}K_x & -K_x\\ -K_x & K_x\end{bmatrix}\left[\mathbf{B}_1\right]+\\ \left[\mathbf{B}_2\right]^T\begin{bmatrix}K_y & -K_y\\ -K_y & K_y\end{bmatrix}\left[\mathbf{B}_2\right]+\\ \left[\mathbf{B}_3\right]^T\begin{bmatrix}K_z & -K_z\\ -K_z & K_z\end{bmatrix}\left[\mathbf{B}_3\right]\end{matrix}\right)d\Omega_e \tag{14}$$

where:

$$\mathbf{B}_1=\begin{bmatrix}\mathbf{B}_x & \\ & \mathbf{B}_x\end{bmatrix}_{2\times 6m},\ \mathbf{B}_2=\begin{bmatrix}\mathbf{B}_y & \\ & \mathbf{B}_y\end{bmatrix}_{2\times 6m},\ \mathbf{B}_3=\begin{bmatrix}\mathbf{B}_z & \\ & \mathbf{B}_z\end{bmatrix}_{2\times 6m} \tag{15}$$

and:

$$\begin{aligned}\mathbf{B}_x&=\begin{bmatrix}\psi_1 & 0 & 0 & \cdots\end{bmatrix}_{1\times 3m},\\ \mathbf{B}_y&=\begin{bmatrix}0 & \psi_1 & 0 & \cdots\end{bmatrix}_{1\times 3m},\\ \mathbf{B}_z&=\begin{bmatrix}0 & 0 & \psi_1 & \cdots\end{bmatrix}_{1\times 3m}\end{aligned} \tag{16}$$

$[K^{IJ}]$ is calculated using 2D Gauss-Legendre quadrature for quadrilateral domains. In the paper, linear (Q4) and quadratic serendipity (Q8) layered quadrilateral elements have been considered. To avoid shear locking, reduced integration is used (2×2 points for Q8 and 1×1 point for Q4 element). The element mass matrix is calculated using the full 2×2 integration, as:

$$\left[M^{IJ}\right]=\int_{\Omega_e}\sum_{I,J=1}^{N}I^{IJ}\mathbf{\Psi}^T\mathbf{\Psi}d\Omega_e \tag{17}$$

where $\mathbf{\Psi}$ is the vector of interpolation (shape) functions.

The mathematical model on the structural level is finally obtained using the well-known assembly procedure.

2.4 Post-computation of stresses

The assumed piecewise linear interpolation of displacement field through the laminate thickness provides discontinuous stresses and strains across the interface between adjacent layers. Once the nodal displacements are obtained, the stresses at the top and bottom interface of every material layer (k) are computed from the constitutive relations (3) (see [35] for details). The interlaminar stresses $\tau_{xz}^{(k)}, \tau_{yz}^{(k)}, \sigma_z^{(k)}$ do not satisfy continuous distribution through the laminate thickness and they are further post-computed by assuming the quadratic distribution within each layer for every stress component. Note that the stress field acting in the CLT and concrete is enriched by adding the interface (int) shear stresses. They are inherited from the displacement jumps Δu and Δv (note that Δw~0) and proportional to the slip moduli K_i:

$$\begin{Bmatrix}\tau_{xz}\\ \tau_{yz}\end{Bmatrix}^{\text{int}}=\begin{bmatrix}K_x & 0\\ 0 & K_y\end{bmatrix}\sum_{j=1}^{m}\begin{bmatrix}\psi_j & 0\\ 0 & \psi_j\end{bmatrix}\begin{Bmatrix}\Delta u_j\\ \Delta v_j\end{Bmatrix} \tag{18}$$

3 Model validation

A validation example considers the rectangular CLT-concrete composite plate with dimensions a×b = 8×7 m [42], with two clamped edges, two free edges and a hinged point support at the corner in point 2, according to Figure 3. CLT has seven layers, with a thickness of (2+4+2+4+2+4+2) = 20 cm, while a concrete topping is 11 cm thick. This corresponds to the a/h ratio of approximately 25 (thin plate situation). The CLT has the following material properties: E_L=12 GPa, E_R=E_T=0.45 GPa, G_{LR}=G_{LT}=0.70 GPa, G_{RT}=0.06 GPa and ν_{LR}=ν_{LT}=ν_{RT}=0.4. For concrete, E_c = 30 GPa and ν_c = 0.2. The layers within a CLT are perfectly bonded, while at the CLT-concrete interface, two combinations of slip moduli K_x and K_y are used (K_x = 1000 MPa and K_x = 10 MPa), keeping the constant ratio K_y/K_x = 2 (K_y = 2000 MPa and K_y = 20 MPa). The composite plate is exposed to the distributed load at the top surface of q_t = 10 kN/m^2.

The plate is discretized using two different mesh densities: 16×14 (element size = 50 cm) and 32×28 elements (element size = 25 cm). Both Q4R and Q8R elements are used, to avoid shear locking due to the spurious transverse shear and normal stiffnesses. The laminas within a CLT are modeled as a single numerical layer, while the concrete layer is modeled using two identical 5.5 cm thick layers - sub-laminate concept (L1). Boundary conditions are prescribed in edge nodes: U^i = V^i = W^i = 0 for clamped edges and W^i = 0 for the hinged point support.

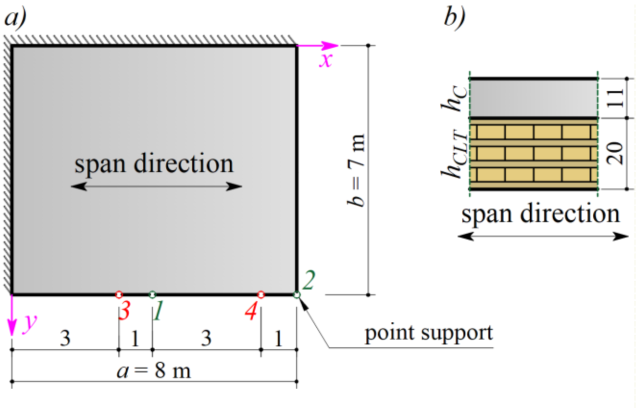

Figure 3. Considered CLT-C composite a × b = 8×7 m, h = 20+11 = 31 cm: a) layout; b) cross-section

The obtained results are compared against the data extracted from [42], obtained using the following models:

– a continuum-based model, generated in Abaqus using C3D20R elements (hexahedral quadratic elements with reduced integration), with three elements across the thickness of each individual layer (L3), and the CLT-concrete interface modeled using cohesive elements COH3D8,

– a Furtmüller's higher-order zig-zag plate theory-based model, accounting for partial interaction between concrete and CLT, generated in MATLAB using Q8 finite elements with reduced integration and nine degrees of freedom (DOFs) per node.

The total number of DOFs introduced in the considered computational models is provided in Table 1.

Figures 4-7 illustrate the distributions of the in-plane displacements *u* and *v* at points 1 (*a/2*, *b*) and 2 (*a*, *b*) through the thickness of the considered CLT-concrete composite. The zig-zag shaped distribution of displacements is achieved by using FLWT for both element types and both considered mesh densities. A minor discrepancy is detected only for a 16×14 mesh of Q4R elements (dashed blue lines in Figures 4-7), which introduces the lowest number of DOFs in all considered scenarios (see Table 1).

Table 1. Properties of computational (finite element) models

Model	Element size	DOFs
FLWTFEM 16×14 Q4R L1	50 cm	8 415
FLWTFEM 16×14 Q8R L1	25 cm	28 587
FLWTFEM 32×28 Q4R L1	50 cm	31 581
FLWTFEM 32×28 Q8R L1	25 cm	92 697
Abaqus C3D20R COH3D8 L3 [42]	0.20 cm	480 156
Higher-order zig-zag theory Q8R [42]	0.20 cm	39 159

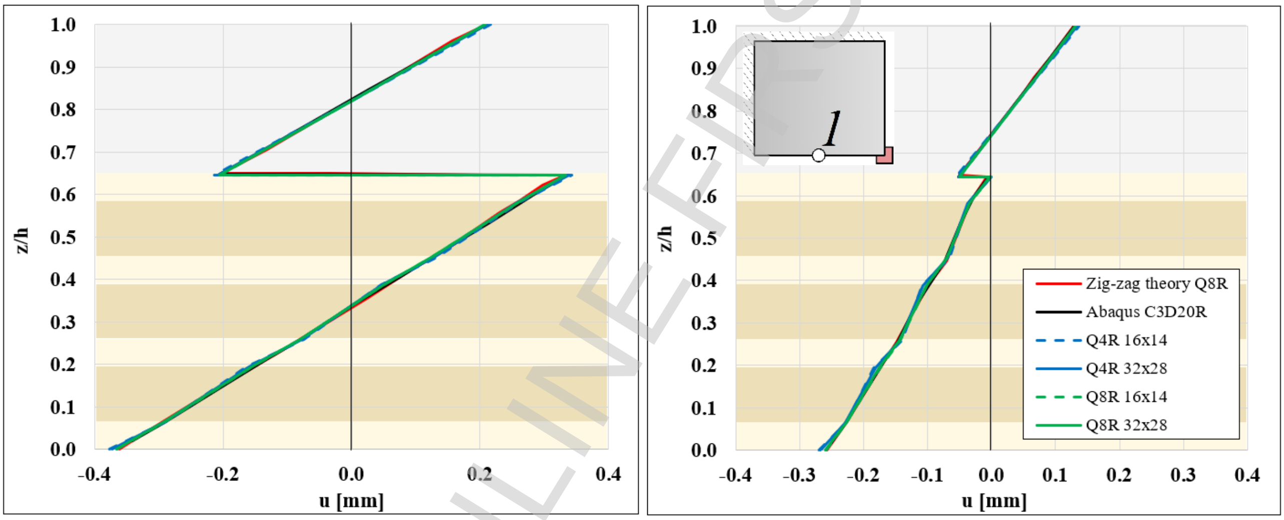

Figure 4. Distributions of the in-plane displacement u(a/2, b) through the thickness of the CLT-concrete composite plate, considering different models and mesh densities. left: K_x = 10 MPa, right: K_x = 1000 MPa

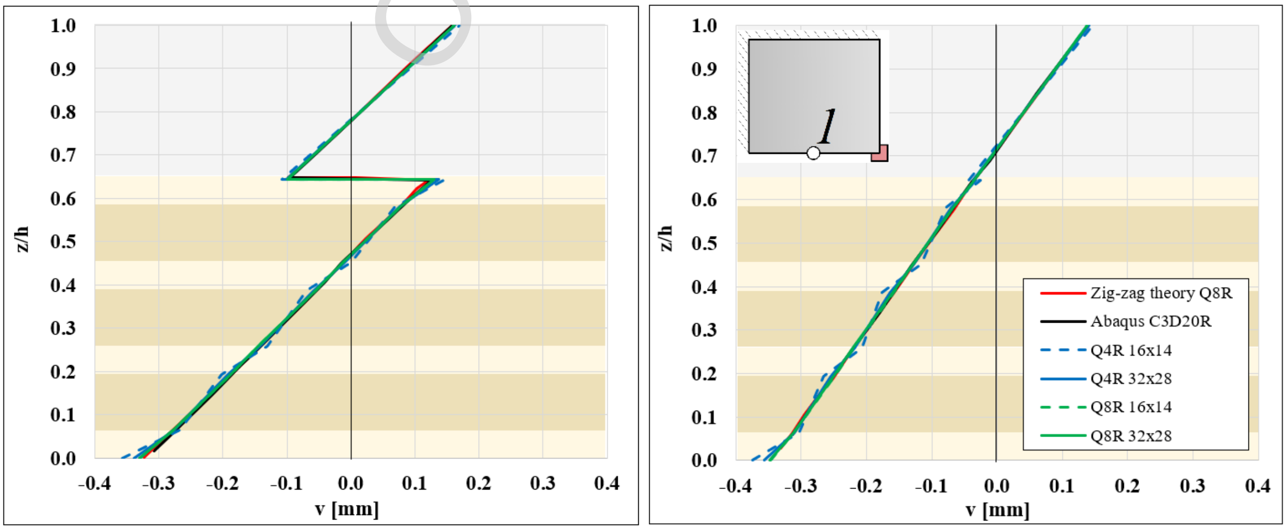

Figure 5. Distributions of the in-plane displacement v(a/2, b) through the thickness of the CLT-concrete composite plate, considering different models and mesh densities. left: K_x = 10 MPa, right: K_x = 1000 MPa

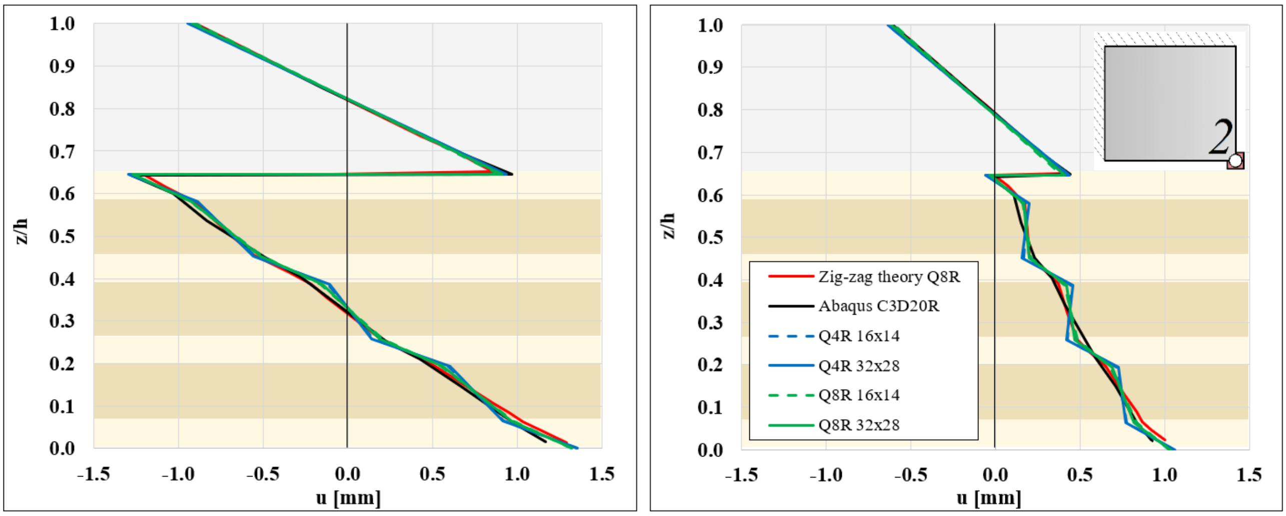

Figure 6. Distributions of the in-plane displacement u(a, b) through the thickness of the CLT-concrete composite plate, considering different models and mesh densities. left: K_x = 10 MPa, right: K_x = 1000 MPa

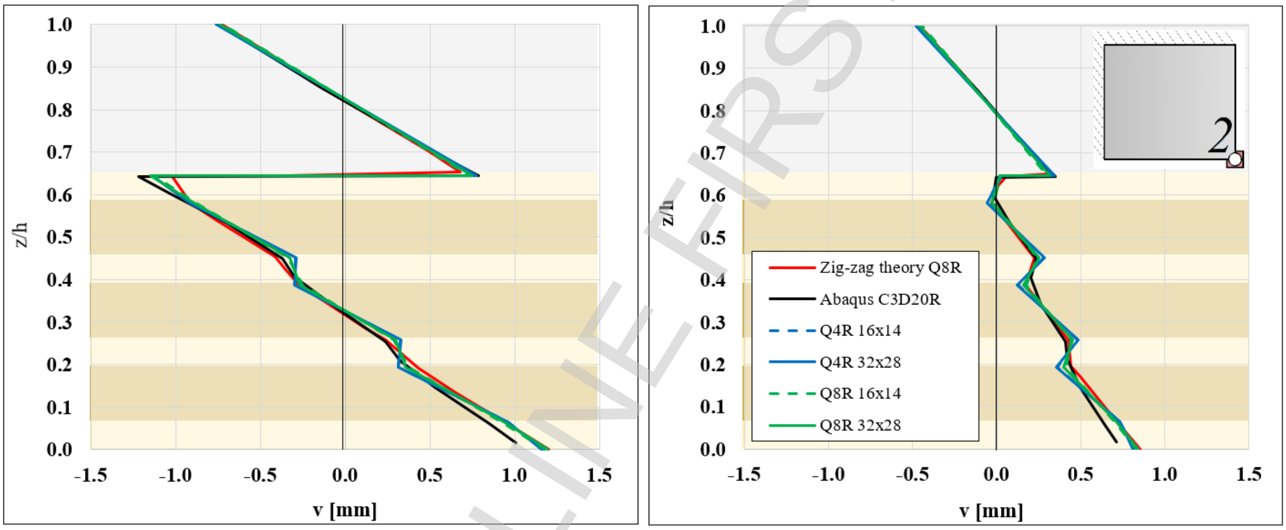

Figure 7. Distributions of the in-plane displacement v(a, b) through the thickness of the CLT-concrete composite plate, considering different models and mesh densities. left: K_x = 10 MPa, right: K_x = 1000 MPa

The values of the inter-layer slip are captured accurately in all models, proving that a proposed layerwise model is capable to accurately predict the kinematics of the CLT-concrete composite with partial shear connection between CLT and concrete. When comparing the results for different slip moduli, it is expectedly obtained that increase of the K_x results in lower interlayer slip, providing higher level of the composite action. Note that $\Delta u(a/2, b)$ and $\Delta v(a/2, b)$ are almost zero for K_x = 1000 MPa (Figures 4-5, right). Excellent agreement is obtained for lateral displacement, too (see Figure 8), for all considered models.

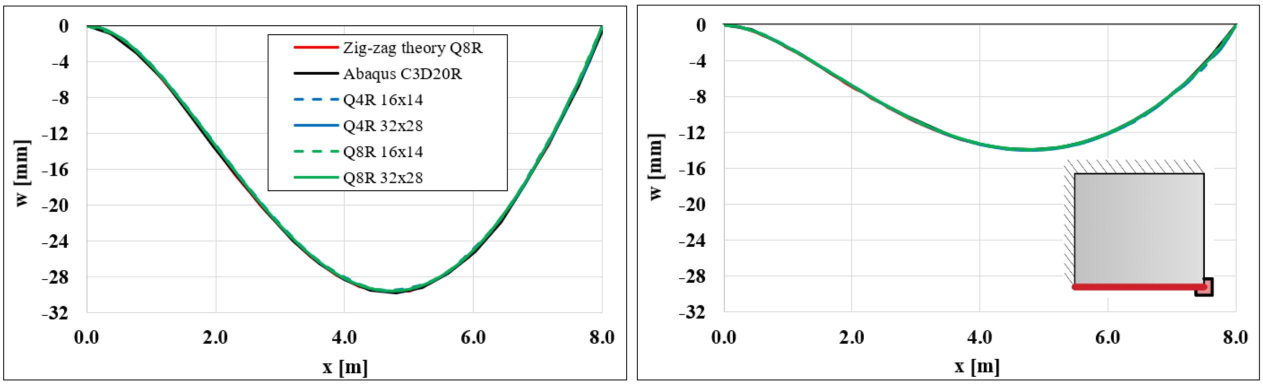

Figure 8. Distributions of the deflection w(x, b) along the bottom free edge of the CLT-concrete la composite plate, considering different models and mesh densities. left: K_x = 10 MPa, right: K_x = 1000 MPa

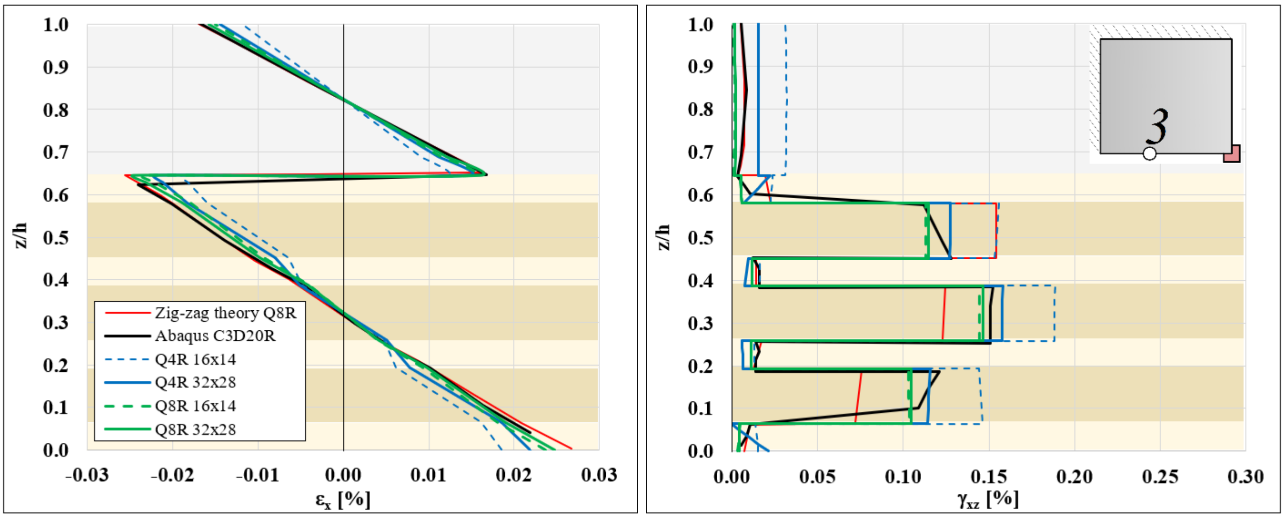

Figure 9. Distributions of the strains in point 3 (3m, b) through the thickness of the CLT-concrete composite plate, considering different models and mesh densities, for K_x = 10 MPa. left: normal strain ε_x, right: transverse shear strain γ_{xz}

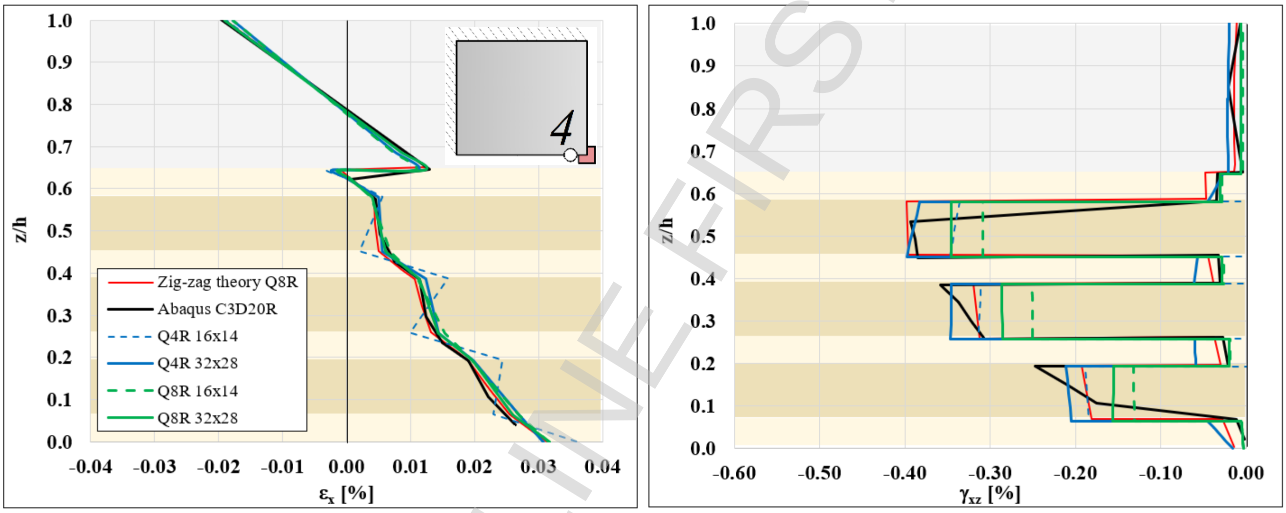

Figure 10. Distributions of the strains in point 4 (7m, b) through the thickness of the CLT-concrete composite plate, considering different models and mesh densities (K_x = 1000 MPa). left: normal strain ε_x, right: transverse shear strain γ_{xz}

Again, the increase of the K_x to 1000 MPa provided the higher level of the composite action, which increased the bending stiffness of the plate and consequently reduced the overall lateral displacements (Figure 8, right) when compared to low interlayer slip modulus K_x = 10 MPa (Figure 8, left).

For all considered models, the strain field obtained by using FLWT is layerwise-linear, because of the layerwise linear expansion of displacements through the plate thickness. Normal strain ε_x in points 3 and 4 (Figure 3) exhibits the laminate-specific zig-zag shape, with discontinuity at CLT-concrete interface. Excellent agreement is achieved when compared with the benchmark data (Figures 9-10, left), with a discrepancy detected only for a 16×14 mesh of Q4R elements (dashed blue lines in Figures 9-10, left). Jumps in the normal strain ε_x are captured accurately in all models. Note that for K_x = 10 MPa (Figure 9, left), CLT and concrete act as almost mutually independent plates, which is visible from the u, v and ε_x distributions across CLT and concrete (Figures 4-7 and 9, left). The proposed model accurately captures the layerwise-stepped distribution of transverse shear strain γ_{xz} (Figures 9-10, right), too. Here, the advantage of the FLWT-based Q8R elements against the Q4R elements is detected, especially when comparing the results from coarse 16×14 meshes. Q4R elements overestimate the transverse shear strain when K_x = 10 MPa, for coarse mesh (Figure 9, right), while better agreement is detected for K_x = 1000 MPa. Finally, for both considered K_x values, transverse shear deformation is 8-10 times higher in CLT when compared to concrete, due to the low shear moduli of timber when compared against G_c.

The above completes the model validation by means of static analysis, since excellent agreement for displacement and strain fields is obtained using the proposed model, with a minor influence of mesh density on the accuracy. Next, a short parametric study is provided to serve as a benchmark for future investigations and illustrate the influence of interlayer slip modulus on stress distribution within CCC composite. For this purpose, the same CCC panel is analyzed and meshed using the 32×28 mesh of Q8R elements which already demonstrated better accuracy for stress field prediction in CLT, especially for transverse shear stresses [35]. The interlayer slip modulus between CLT and concrete has been varied, ranging from 1 kPa (simulating the absence of any connection between CLT and concrete – red line in Figure 11) to 1000 MPa (simulating the approximately

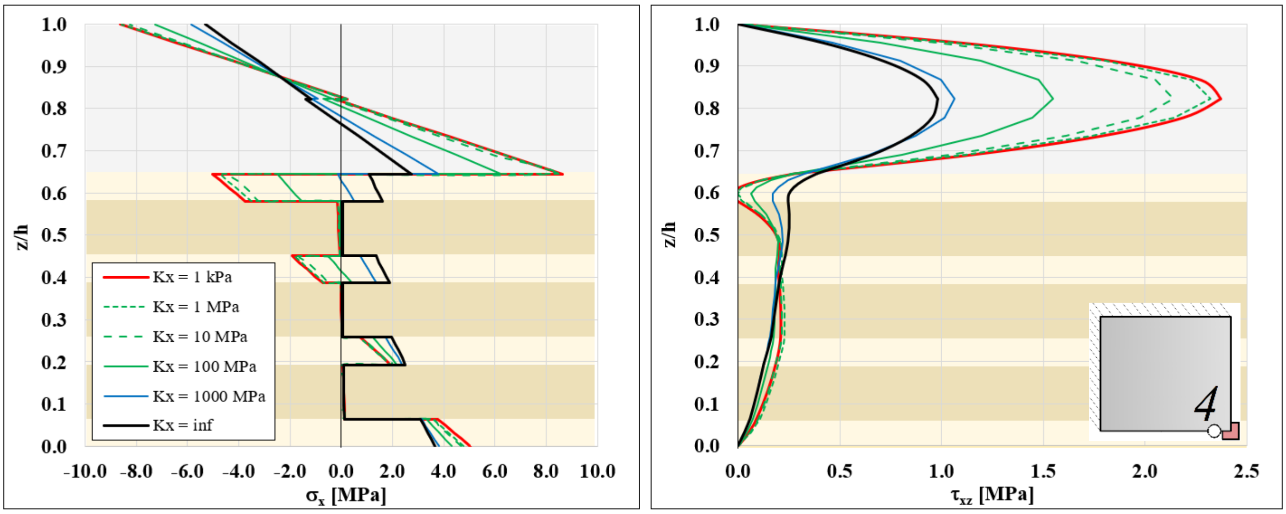

Figure 11. Distributions of the stresses in point 4 (7m, b) through the thickness of the CLT-concrete composite plate, considering different stiffnesses K_x, for 32×28 mesh of Q8R finite elements. left: normal stress σ_x, right: transverse shear stress τ_{xz}

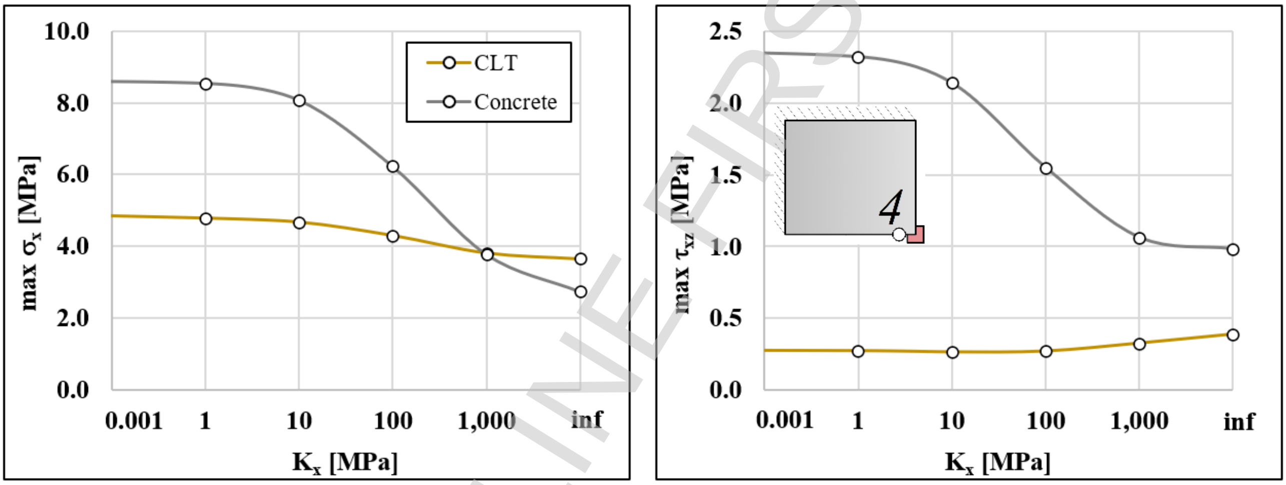

Figure 12. Influence of the interface stiffness K_x on the stress distributions in point 4 (7m, b) through the thickness of the CLT-concrete composite plate, for 32×28 mesh of Q8R finite elements. left: normal stress σx, right: shear stress τ_{xz}

perfect shear connection). A model with perfect bonding of all layers [35] is used as an upper bound benchmark (black line in Figure 11). In all simulations, $K_y/K_x = 2$ ratio is adopted.

Figure 11 shows the normal (σ_x) and transverse shear stress (τ_{xz}) distributions through the thickness of the CLT-concrete composite plate, considering different CLT-concrete interface stiffnesses K_x. The increase of K_x contributes to the composite action between CLT and concrete, resulting in the reduction of the interlayer slip and consequently the reduction in maximum stresses in the concrete layer (grey line in Figure 12). The slight reduction of the maximum normal stress (orange line in Figure 12, left) and minor increase of the maximum shear stress (orange line in Figure 12, right) is detected in CLT.

In the second part of the validation example, free vibration study of the considered composite plate has been conducted. For this purpose, only the self-weight of the structure has been considered as a mass source (ρ_{CLT} = 420 kg/m^3 and ρ_c = 2500 kg/m^3). The obtained results are again compared against the data [42], obtained using the Abaqus continuum-based model (C3D20R and COH3D8), and the Furtmüller's higher-order zig-zag plate theory-based model with partial interaction. The total number of DOFs in the following simulations corresponds to those given in Table 1.

Obtained natural frequencies with corresponding differences relative to the zig-zag theory [42] are given in Tables 2-3 and illustrated in Figure 13, while the comparison of the first 10 mode shapes is illustrated in Figure 14 (for K_x = 10 MPa). The results presented in Tables 2-3 and Figures 13-14 clearly show the high accuracy of the proposed model in the prediction of natural frequencies and mode shapes of CCC with different interlayer slip moduli. Only the coarse 16×14 mesh of Q4R elements, which includes 4.65 times less DOFs then the benchmark example showed the slight discrepancy in obtained natural frequency (the average relative differences are +1.4% for K_x = 10 MPa and +1.7% for K_x = 1000 MPa). For other scenarios, the average relative differences are ranging from -0.7% to +0.4%, which is almost negligible.

The above completes the model validation by means of free vibration study, since excellent agreement is obtained when compared with the benchmark data. Obviously, the model accurately simulates the stiffness and mass distribution in CCC and consequently provides the reliable data by means of natural frequencies and mode shapes.

Table 2. Natural frequencies of the CLT-concrete composite plate, considering different computational models and mesh densities (K_x = 10 MPa)

Mode	Zig-zag theory Q8R [42]	Abaqus C3D20R [42]	Q4R 16x14	Q4R 32x28	Q8R 16x14	Q8R 32x28
1	6.0	6.0	$6.04^{+0.7\%}$	$6.02^{+0.3\%}$	$6.02^{+0.3\%}$	$6.01^{+0.2\%}$
2	10.4	10.4	$10.46^{+0.5\%}$	$10.39^{-0.1\%}$	$10.38^{-0.2\%}$	$10.37^{-0.2\%}$
3	15.1	15.0	$15.15^{+0.3\%}$	$15.04^{-0.4\%}$	$15.02^{-0.6\%}$	$15.01^{-0.6\%}$
4	20.3	20.2	$20.57^{+1.4\%}$	$20.31^{\pm 0.0\%}$	$20.24^{-0.3\%}$	$20.23^{-0.3\%}$
5	25.3	25.0	$25.65^{+1.4\%}$	$25.19^{-0.4\%}$	$25.07^{-0.9\%}$	$25.06^{-1.0\%}$
6	29.6	29.2	$30.00^{+1.3\%}$	$29.49^{-0.4\%}$	$29.33^{-0.9\%}$	$29.32^{-0.9\%}$
7	32.8	32.3	$33.10^{+0.9\%}$	$32.54^{-0.8\%}$	$32.39^{-1.3\%}$	$32.38^{-1.3\%}$
8	38.2	37.7	$39.15^{+2.5\%}$	$38.12^{-0.2\%}$	$37.85^{-0.9\%}$	$37.82^{-1.0\%}$
9	43.4	42.8	$44.56^{+2.7\%}$	$43.36^{-0.1\%}$	$43.01^{-0.9\%}$	$42.99^{-1.0\%}$
10	47.2	46.6	$48.13^{+2.0\%}$	$47.06^{-0.3\%}$	$46.75^{-0.9\%}$	$46.73^{-1.0\%}$

Table 3. Natural frequencies of the CLT-concrete composite plate, considering different computational models and mesh densities (K_x = 1000 MPa)

Mode	Zig-zag theory Q8R [42]	Abaqus C3D20R [42]	Q4R 16x14	Q4R 32x28	Q8R 16x14	Q8R 32x28
1	9.0	9.0	$9.05^{+0.6\%}$	$9.02^{+0.2\%}$	$9.03^{+0.4\%}$	$9.03^{+0.3\%}$
2	15.7	15.8	$15.81^{+0.7\%}$	$15.72^{+0.2\%}$	$15.71^{+0.1\%}$	$15.70^{\pm 0.0\%}$
3	21.7	21.7	$21.87^{+0.8\%}$	$21.73^{+0.1\%}$	$21.73^{+0.1\%}$	$21.72^{+0.1\%}$
4	27.9	28.0	$28.25^{+1.3\%}$	$27.99^{+0.3\%}$	$27.94^{+0.1\%}$	$27.93^{+0.1\%}$
5	34.2	34.2	$34.79^{+1.7\%}$	$34.32^{+0.3\%}$	$34.24^{+0.1\%}$	$34.22^{+0.1\%}$
6	40.9	41.0	$41.65^{+1.8\%}$	$41.14^{+0.6\%}$	$40.98^{+0.2\%}$	$40.97^{+0.2\%}$
7	44.4	44.4	$45.35^{+2.1\%}$	$44.61^{+0.5\%}$	$44.43^{+0.1\%}$	$44.41^{\pm 0.0\%}$
8	49.4	49.4	$50.66^{+2.5\%}$	$49.66^{+0.5\%}$	$49.38^{\pm 0.0\%}$	$49.36^{-0.1\%}$
9	54.5	54.5	$56.17^{+3.1\%}$	$54.87^{+0.7\%}$	$54.56^{+0.1\%}$	$54.52^{\pm 0.0\%}$
10	59.5	59.5	$60.64^{+1.9\%}$	$59.78^{+0.5\%}$	$59.51^{\pm 0.0\%}$	$59.49^{\pm 0.0\%}$

4 Conclusions

Starting from the full-layerwise-plate-theory-based FEM formulation for laminated composite plates with perfect bonding, the paper extends the formulation to account for the possible interlayer slip. This phenomenon is common in CLT-concrete and other plate-like composites with mechanical couplers. Therefore, a CLT-concrete composite plate is considered for model validation. The interface slip moduli are incorporated using the smeared approach, as distributed linear springs at the interface. Interlayer slips are introduced by means of different displacements at the interface numerical layers. This is enabled by using the discontinuous interpolation functions of the thickness coordinate, previously developed for delamination studies. The strain field is enriched by adding the singularity terms related to the CLT-concrete interface. The stress field is enriched by adding the interface shear stress contributions inherited from the displacement jumps and proportional to the interlayer slip moduli.

Based on the presented formulation, Q4 and Q8 layered quadrilateral isoparametric finite elements have been developed. They provide the complete stress/strain fields necessary for engineering failure analysis, delamination studies or stress-deformation state around point supports. The model is rotation-free and requires only C^0 continuity of

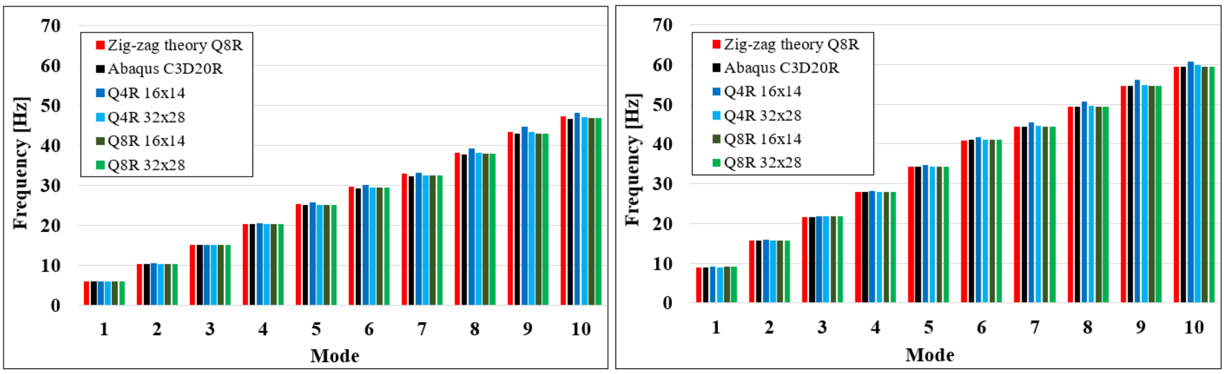

Figure 13. Natural frequencies of the CLT-concrete composite plate, considering different computational models and mesh densities. left: K_x = 10 MPa, right: K_x = 1000 MPa

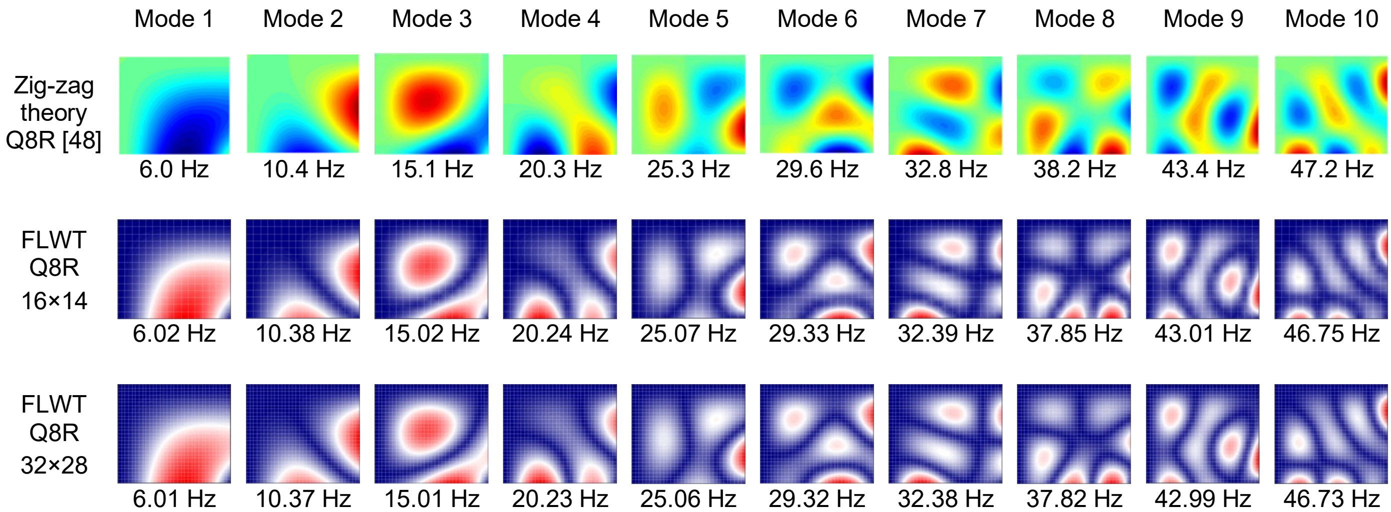

Figure 14. Mode shapes of the CLT-concrete composite plate, considering different mesh densities of Q8R finite elements (K_x = 10 MPa)

generalized displacements along element boundaries.

The thickness coordinate is eliminated by the explicit integration of stress components; thus, a model formulation is reduced to the 2D (plate) model without compromising the accuracy and providing the computational cost savings when compared against the continuum-based (solid) models. Finally, the model allows the analysis of timber-concrete (TCC) or other plate-like layered composites with partial shear connection and arbitrary geometry.

From the conducted computational analysis, the following conclusions are derived:

- The zig-zag shaped distribution of displacement u, which is in accordance with the exact solution, is achieved for both linear and quadratic layered finite elements. The values of the inter-layer slip and lateral displacement are captured accurately in all considered scenarios, proving that a proposed model accurately predicts the kinematics of the CLT-concrete composite with partial shear connection. The increase of the slip modulus expectedly resulted in lower interlayer slip.
- Both elements predicted the layerwise-linear strain field. Normal strain ε_x exhibits the laminate-specific zig-zag shape, with discontinuity at CLT-concrete interface, while the transverse shear strain γ_{xz} exhibits the jumps at layer interfaces. Excellent agreement is achieved when compared with the benchmark data, with a discrepancy detected only for a relatively coarse mesh of Q4R elements.
- The benchmark study showed that the increase of the slip modulus leads to the reduction in maximum stresses in the concrete layer, with the slight reduction of the maximum normal stress and minor increase of the maximum shear stress in CLT.
- The model provided the high accuracy in the prediction of natural frequencies and mode shapes of CLT-concrete composite plate with various slip moduli, with the average relative difference less than 1%. Only the coarse 16×14 mesh of Q4R elements showed the slight discrepancy, with +1.4% difference for K_x = 10 MPa and +1.7% for K_x = 1000 MPa.

CRediT authorship contribution statement

Conceptualization – M.M.; Formal analysis – M.M.; Investigation – M.M.; Methodology – M.M.; Software – M.M.; Validation – M.M.; Visualization – M.M.; Writing - original draft – M.M.; Writing - review & editing – M.M.

Declaration of competing interest

The author declares no competing interest that could inappropriately influence the research presented in this work.

Acknowledgments

The financial support of the Ministry of Education, Science and Technological Development of the Republic of Serbia, through the project 200092 is acknowledged. The author is grateful to Dr. Emilija Jočić for her contribution in development of the FLWTFEM software.

References

[1] R. Brandner, G. Flatscher, A. Ringhofer, G. Schickhofer, A. Thiel, Cross laminated timber (CLT): overview and development, Eur. J. Wood Wood Prod. 74 (2016) 331–51. https://doi.org/10.1007/s00107-015-0999-5

[2] R. Brandner, Production and Technology of Cross Laminated Timber (CLT): State-of-the-Art Report, Focus Solid Timber Solutions – European Conference on Cross Laminated Timber (CLT), Graz, Austria, 2013.

[3] G. Fink, J. Kohler, R. Brandner, Application of European design principles to cross laminated timber, Eng. Struct. 171 (2018) 934-943. https://doi.org/10.1016/j.engstruct.2018.02.081

[4] A. Siddika, A. Al Mamun, F. Aslani, Y. Zhuge, R. Alyousef, A. Hajimohammadi, Cross-laminated timber–concrete composite structural floor system: A state-of-the-art review, Eng. Fail. Anal. 130 (2021) 105766. https://doi.org/10.1016/j.engfailanal.2021.105766

[5] M. Shahnewaz, R. Jackson, T. Tannert, Reinforced cross-laminated timber-concrete composite floor systems, Eng. Struct. 291 (2023) 116395. https://doi.org/10.1016/j.engstruct.2023.116395

[6] A. Forsberg, F. Farbäck, Timber concrete composite floors with cross laminated timber - structural behavior & design, Report TVBK-20/5279, Lund University, 2020.

[7] Dias, J. Skinner, K. Crews, T. Tannert, Timber-concrete-composites increasing the use of timber in construction, Eur. J. Wood Wood Prod. 74(3) (2016) 443–451. https://doi.org/10.1007/s00107-015-0975-0

[8] D. Yeoh, M. Fragiacomo, M. De Franceschi, K. Heng Boon, State of the Art on Timber-Concrete Composite Structures: Literature Review, J. Structu. Eng. 137(10) (2011) 1085–1095.

[9] A. Ceccotti, Composite concrete-timber structures, Prog. Struct. Eng. Mater. 4(3) (2002) 264-275. https://doi.org/10.1002/pse.126

[10] Q. Xu, M. Wang, L. Chen, K. A. Harries, X. Song, Z. Wang, Mechanical performance of notched shear connections in CLT-concrete composite floor, J. Build. Eng. 70 (2023) 106364. https://doi.org/10.1016/j.jobe.2023.106364

[11] Y. Jiang, R. Crocetti, CLT-concrete composite floors with notched shear connectors, Const. Build. Mater. 195 (2019) 127-139. https://doi.org/10.1016/j.conbuildmat.2018.11.066

[12] L. Boccadoro, S. Zweidler, R. Steiger, A. Frangi, Bending tests on timber-concrete composite members made of beech laminated veneer lumber with notched connection, Eng. Struct. 132 (2017) 14–28. https://doi.org/10.1016/j.engstruct.2016.11.029

[13] S. R. S. Monteiro, A. M. P. G. Dias, J. H. J. O. Negrão, Assessment of Timber-Concrete Connections Made with Glued Notches: Test Set-Up and Numerical Modeling. Exp. Tech. 37 (2013) 50-65.

[14] J. Skinner, J. Bregulla, R. Harris, K. Paine, P. Walker, Screw connectors for thin topping, timber–concrete composites, Mater. Struct. 47 (2014) 1891-1899. https://doi.org/10.1617/s11527–013–0158–6

[15] M. A. H. Mirdad, Y. H. Chui, Load–slip performance of Mass Timber Panel–Concrete (MTPC) composite connection with Self–tapping screws and insulation layer, Const. Build. Mater. 213 (2019) 696-708. https://doi.org/10.1016/j.conbuildmat.2019.04.117

[16] A.M. P. G. Dias, S. M. R. Lopes, J. W. G. Van de Kuilen, H. M. P. Cruz, Load-Carrying Capacity of Timber–Concrete Joints with Dowel-Type Fasteners, J. Struct. Eng. 33 (2007) 720–727. https://doi.org/10.1061/(ASCE)0733-9445(2007)133:5(720)

[17] M. Brunner, M. Romer, M. Schnüriger, Timber-concrete-composite with an adhesive connector (wet on wet process), Mater. Struct. 40(1) (2007) 119-126. https://doi.org/10.1617/s11527-006-9154-4

[18] J. Kanócz, V. Bajzecerová, Analysis of composite action of various mass timber structural panels with concrete layer, Wood Res. 63 (2018) 1091-1100.

[19] S. C. Auclair, L. Sorelli, A. Salenikovich, A new composite connector for timber-concrete composite structures. Const. Build. Mater. 112 (2016) 84-92. https://doi.org/10.1016/j.conbuildmat.2016.02.025

[20] M. Wang, Q. Xu, K. A. Harries, L. Chen, Z. Wang, X. Chen, Experimental study on mechanical performance of shear connections in CLT-concrete composite floor, Eng. Struct. 269 (2022) 114842. https://doi.org/10.1016/j.engstruct.2022.114842

[21] K. Q. Mai, A. Park, K. Lee, Experimental and numerical performance of shear connections in CLT–concrete composite floor, Mater. Struct. 51 (2018) 1-13. https://doi.org/10.1617/s11527–018–1202–3

[22] J. Cao, H. Xiong, Z. Wang, J. Chen, Experimental investigation and numerical analysis for concrete-CLT connections, Const. Build. Mater. 236 (2020) 117533. https://doi.org/10.1016/j.conbuildmat.2019.117533

[23] E. Lukaszewska, H. Johnsson, M. Fragiacomo, Performance of connections for prefabricated timber-concrete composite floors. Mater. Struct. 41(9) (2008) 1533-1550. https://doi.org/10.1617/s11527-007-9346-6

[24] J. Cao, H. Xiong, J. Chen, Mechanical characteristics and analytical model of CLT-concrete composite connections under monotonic loading, Const. Build. Mater. 335 (2022) 127472. https://doi.org/10.1016/j.conbuildmat.2022.127472

[25] G. Y. Jeong, V. S. Pham, D. K. Tran, Development of predicting equations for slip modulus and shear capacity of CLT–concrete composite with screw connections, J. Build. Eng. 71 (2023) 106468.

[26] M. Milojević, V. Racic, M. Nefovska-Danilović, Uncertainty analysis of CLT floor vibrations due to inherent variability in structural properties. J. Build. Eng. 113 (2025) 113725. https://doi.org/10.1016/j.jobe.2025.113725

[27] A. Aloisio, D. Pasquale Pasca, Y. De Santis, T. Hillberger, P. Francesco Giordano, M. Martino Rosso, R. Tomasi, M. Pina Limongelli, C. Bedon, Vibration issues in timber structures: A state-of-the-art review, J. Build. Eng. 76 (2023) 107098. https://doi.org/10.1016/j.jobe.2023.107098

[28] V. Racic, Emerging research on vibration serviceability assessment of pedestrian structures, Build. Mater. Struct. 66(2) (2023) 85-92. https://doi.org/10.5937/grmk2300001r

[29] E. Ussher, K. Arjomandi, I. Smith, Status of vibration serviceability design methods for lightweight timber floors, J. Build. Eng. 50 (2022) 104111. https://doi.org/10.1016/j.jobe.2022.104111

[30] D. Casagrande, I. Giongo, F. Pederzolli, A. Franciosi, M. Piazza, Analytical, numerical and experimental assessment of vibration performance in timber floors, Eng. Struct. 168 (2018) 748-758. https://doi.org/10.1016/j.engstruct.2018.05.020

[31] A. S. Mohammed, A. Pavic, V. Racic, Improved model for human induced vibrations of high-frequency floors, Eng. Struct. 168 (2018) 950-966. https://doi.org/10.1016/j.engstruct.2018.04.093

[32] C. Guo, J. Zhou, Y. H. Chui, Experimental and numerical investigations on vibration performance of mass timber slab floors with floating concrete toppings, Eng. Struct. 330 (2025) 119919. https://doi.org/10.1016/j.engstruct.2025.119919

[33] Y. Bao, Y. Han, Z. Xu, W. Lu, K. Yue, B. Lu, Vibration performance of cross-laminated timber (CLT)-concrete composite floors considering the section thickness ratio between CLT panels and concrete slabs, Eng. Struct. 340 (2025) 120783. https://doi.org/10.1016/j.engstruct.2025.120783

[34] S. Malek, N. Cheraghi-shirazi, A. Creagh, F. Setiawan, R. Parra, P. Khoshkbari, Vibration performance of CLT and CLT-concrete composite floors supported by glulam beams under human activity in mass timber office buildings, Eng. Struct. 330 (2025) 119918. https://doi.org/10.1016/j.engstruct.2025.119918

[35] M. Marjanović, N. Marković, E. Damnjanović, R. Cvetković, Three-dimensional stress analysis and design of cross-laminated timber panels using full-layerwise-theory-based finite element method, Thin-Walled Struct. 157 (2020) 107–156. https://doi.org/10.1016/j.tws.2020.107156

[36] G. Kirchhoff. Über das Gleichgewicht und die Bewegung einer elastischen Scheibe, J. Reine Angew. Math. 40 (1850) 51-88.

[37] E. Reissner, The effect of transverse shear deformation on the bending of elastic plates. J. Appl. Mech. 12(2) (1945) 69-79.

[38] R. Mindlin, Influence of rotator inertia and shear in flexural motions of isotropic elastic plates, J. Appl. Mech. 18(1) (1951) 1031-1038.

[39] J. N. Reddy, A simple higher-order theory for laminated composite plates, J. Appl. Mech. 51 (1984) 745-752.

[40] T. Furtmüller, C. Adam, An accurate higher order plate theory for vibrations of cross-laminated timber panels, Compos. Struct. 239 (2020) 112017. https://doi.org/10.1016/j.compstruct.2020.112017

[41] J. Whitney, Shear correction factors for orthotropic laminates under static load, J. Appl. Mech. 40(1) (1973) 302-304. https://doi.org/10.1115/1.3422950

[42] T. Furtmüller, A finite element for static and dynamic analyses of concrete–cross-laminated timber composite plates, Eng. Struct. 328 (2025) 119704. https://doi.org/10.1016/j.engstruct.2025.119704

[43] S. G. Lekhnitskii, Strength calculation of composite beams, Vestnik Inzhen I Teknikov 9 (1935) 137–148.

[44] J. Ren, A new theory of laminated plate, Compos. Sci. Tech. 26 (1986) 225–239. https://doi.org/10.1016/0266-3538(86)90087-4

[45] R. Stürzenbecher, K. Hofstetter, Bending of cross-ply laminated composites: An accurate and efficient plate theory based upon models of Lekhnitskii and Ren, Compos. Struct. 93 (2011) 1078–88. https://doi.org/10.1016/j.compstruct.2010.09.020

[46] T. Furtmüller, C. Adam, A linear finite element for timber–concrete layered beams with interlayer slip, Compos. Struct. 316 (2023), 117045. https://doi.org/10.1016/j.compstruct.2023.117045

[47] D. Ladurner, C. Adam, T. Furtmüller, Geometric nonlinear analysis of slender layered non-prismatic beams with interlayer slip, Int. J. Mech. Sci. 261 (2024) 108651. https://doi.org/10.1016/j.ijmecsci.2023.108651

[48] J. N. Reddy, Mechanics of laminated composite plates and shells: theory and analysis, CRC Press, Boca Raton, Florida, USA, 2004.

[49] E. Jočić, M. Todorović, I. Glišović, M. Marjanović, An efficient computational model for progressive failure analysis of cross-laminated timber panels, Arch. Appl. Mech. 95 (2025) 155. https://doi.org/10.1007/s00419-025-02868-7

[50] https://github.com/miregrf/FLWTFEM

[51] M. Marjanovic, G. Meschke, E. Damnjanovic, Object-oriented framework for 3D bending and free vibration analysis of multilayer plates: Application to cross-laminated timber and soft-core sandwich panels, Compos. Struct. 255 (2021) 112–159. https://doi.org/10.1016/j.compstruct.2020.112859

[52] MATLAB R2011b, The MathWorks, Inc., Natick, Massachusetts, USA.

[53] GiD Customization Manual. CIMNE – International Center for Numerical Methods in Engineering, 2016.

[54] ABAQUS User Manual 6.9. DS SIMULIA Corp., Providence, Rhode Island, USA, 2009.

[55] M. Rakocevic, L. Zugic. A New Approach to the Embedding of Delamination in the Layerwise Theory of Laminated Composite Plates, Symmetry 14 (2022) 1583. https://doi.org/10.3390/sym14081583